A High-Resolution GSO-based Brain PET Camera

J.S. Karp[1], *Senior Member IEEE*, L.E. Adam[1], R.Freifelder[1], *Member IEEE*, G. Muehllehner[3] *Senior Member IEEE,* F. Liu[1,2], *Student Member IEEE* , S. Surti[1,2], *Student Member IEEE*
Department of [1]Radiology and [2]Physics, University of Pennsylvania, and [3]ADAC UGM, Philadelphia PA

ABSTRACT

A high-resolution GSO-based PET camera is being developed for brain imaging. The system is based upon a detector that uses Anger-logic positioning with 4 x 4 x 10 mm^3 crystals coupled to a continuous light-guide and an array of 39-mm diameter photo-multiplier tubes. Measurements of a small crystal array have demonstrated that individual crystals can be resolved. The system is 3D (no septa) with a diameter of 42 cm and an axial field-of-view of 25 cm. The detector and overall scanner design has been guided by Monte Carlo simulations. The GSO PET scanner will have improved spatial resolution and higher count-rate capability than the NaI(Tl) HEAD Penn-PET scanner that was built previously. GSO was chosen because of its higher stopping power, faster decay, and excellent energy resolution, which is critical for good scatter rejection.

1. INTRODUCTION

A GSO-based PET camera is being developed for brain imaging. The intended applications include research studies using ^{11}C-tagged radio-ligands for neuro-receptor imaging protocols, as well as clinical ^{18}F-FDG studies. The new PET scanner will have improved spatial resolution, higher sensitivity and higher count-rate capability than the NaI(Tl)-based HEAD Penn-PET scanner that we built previously [1,2]. The improved performance will lead to better image quality and/or shorter scan times, and allow more optimal imaging of isotopes with short half-lives.

In keeping with our previous instrumentation development, we will retain much of the design of the detector, electronics, and methods of position processing that are incorporated in the NaI(Tl)-based scanner, but will take advantage of the characteristics of Cerium-doped Gadolinium Orthosilicate, GSO(Ce) [3]. Compared to NaI(Tl), GSO has about a factor of two higher stopping power (μ = 0.67/cm vs. 0.34/cm), much faster decay time (τ = 65 ns vs. 240 ns), but lower light output (about 35% of NaI(Tl)). However, with NaI(Tl), we normally clip the pulse and integrate for only 200 ns, thereby using less than 60% of the total. GSO has previously been investigated as early as 1985 [4] for application to PET as an alternative to BGO, or in combination with BGO [5]. However, for the 2D PET systems being developed in the mid-1980's, the improved timing and energy resolution of GSO compared to BGO were not as critical. Today, LSO rather than GSO is considered by many to be a potential replacement for BGO in today's state-of-the-art 3D PET systems, once the cost of the scintillator decreases. While LSO has slightly superior performance to GSO, LSO is difficult to obtain and very costly. In addition, the LSO crystals being produced at this time have considerable variability in the light output [6], which makes it difficult to obtain good system energy resolution. Since our new PET scanner has a large axial field-of-view (FOV) without septa, we require good scanner energy resolution to minimize scattered radiation and to enable post-injection transmission scanning using ^{137}Cs, in a similar manner as the NaI(Tl)-based HEAD Penn-PET scanner.

2. DETECTOR PERFORMANCE

We performed energy resolution measurements with GSO(Ce) (0.5 mol%) and compared these results to NaI(Tl) and LGSO (90% Lutetium and 10% Gadolinium), which has very similar properties to LSO. Both the LGSO and GSO crystals were made by Hitachi Chemical Co, cut to 4 x 4 x 10 mm^3 and polished using chemical etching [7]. They were wrapped with teflon and grease-coupled to a 39-mm PMT. Using charge integrating ADCs with an integration time of 200 ns, we measured 14% (FWHM) at 511 keV with LGSO and 10% with GSO. Note that GSO has only about one-half the light output of LGSO which affects the PMT Poisson fluctuations, but the intrinsic resolution is much better [8]. In fact, the measured energy resolution of GSO is the same as we measure with NaI(Tl), with pulse clipping and 200 ns integration.

Guided by Monte Carlo computer simulations [9], the detector consists of 4 x 4 x 10 mm^3 crystals on a continuous light-guide, coupled to a hexagonal array of 39-mm photo-multiplier tubes (PMTs). In contrast to the continuous NaI(Tl) detector, this arrangement uses discrete crystals, but still takes full advantage of Anger-type light sharing with a relatively small number of PMTs, thus minimizing the total cost of the system. We chose the 39-mm PMT based on cost considerations (for a complete scanner) and count-rate requirements. This detector configuration using discrete crystals on a continuous light guide is similar to the PCR-II scanner [10], although their system required much smaller PMTs (13-mm diameter) because of the lower light output of the BGO detectors.

Figure 1 shows a schematic of the detector module. The PMTs are arranged in a hexagonal, close-packed pattern. The crystals are accurately positioned with 4.3 mm spacing using a grid made of white silicone RTV with thin walls (0.3mm). Although bench-top measurements were taken with a flat light-guide (UVT lucite), the light-guide for the cylindrical scanner will be curved. Based upon our experience with curved NaI(Tl) detectors and light-guides, we do not expect the curved light-guide for the GSO scanner to cause any difficulties or loss of performance.

Figure 2 (bottom) is a representative 2-D plot of a 50-crystal array (5 x 10). An open flood source of 511 keV gamma rays irradiated the detector. These data were acquired with a 19-mm thick light-guide. Based upon the computer simulations [9], and confirmed by experimental measurements, this thickness was determined to be optimal for crystal identification, using a group of 7 PMTs for position determination. The light spread is controlled by 5-mm deep slots cut into the light-guide face which is coupled to the

0-7803-5696-9/00/$10.00 (c) 2000 IEEE

crystals. The slots reduce the tails of the light response function (LRF), which improves event positioning, and minimizes event pile-up at high count-rates. The average peak/valley ratio of the data in Figure 2 is about 3:1, ranging from 2:1 near the center of this array (positioned over the center of a PMT), to about 4:1 at the edge of this array (positioned between two PMTs).

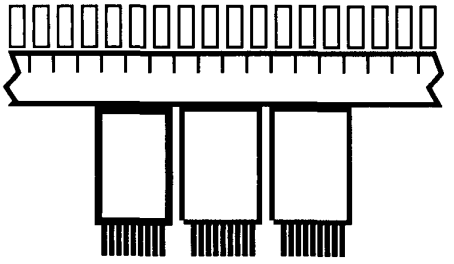

Figure 1. Schematic of GSO detector, with 4 x 4 x 10 mm^3 crystals (not to scale) arranged on a continuous light-guide and coupled to a hexagonal array of 39-mm PMTs.

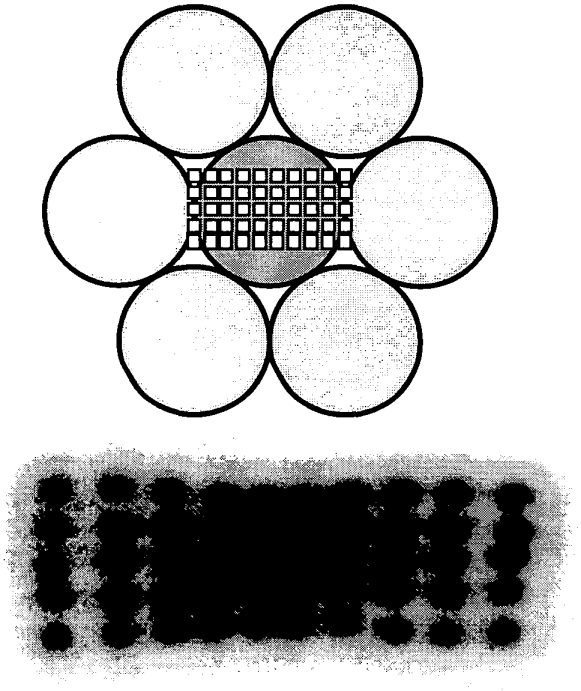

Figure 2. (Top) Schematic of experimental set-up with a 50-crystal array coupled to 7 PMTs (39-mm) with 19-mm thick light-guide. (Bottom) Data from open flood source irradiating GSO detector.

3. SCANNER DESIGN

The crystals were chosen to be relatively short (10 mm) to limit the cost and to minimize parallax in a system with a small diameter. Rather than using 'extra' crystal material for thicker crystals, we use extra crystals to extend the axial FOV to 25 cm. For a 3D system without septa, this leads to a high sensitivity and enhances the flexibility for a variety of imaging situations. While the interaction efficiency (about 57%) of 10-mm thick GSO is similar to that of 19-mm thick NaI(Tl) used in HEAD Penn-PET scanner), the photo-fraction of the GSO is 50% higher. Thus, we can expect a factor of two improvement in coincidence sensitivity, relative to the HEAD Penn-PET [1] (with the same 25-cm axial FOV), yielding about 1.2 Mcps/μCi/cc for the standard NEMA phantom.

A schematic of the complete system is shown in Figure 3. The system diameter and axial FOV are similar to that of the NaI(Tl)-based brain scanner; with 42-cm diameter and 25-cm axial FOV. This requires a total of 18,560 crystals and 288 PMTs. The patient port is 30-cm diameter, with a 6-cm wide ring of shielding used to reject activity outside the FOV.

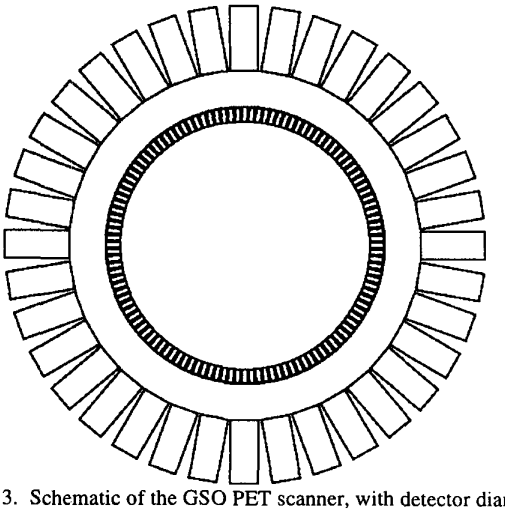

Figure 3. Schematic of the GSO PET scanner, with detector diameter of 42 cm and axial field-of-view of 25 cm. A total of 288 PMTs (36 columns by 8 rows) are coupled to a continuous light-guide, with 18,560 crystals (320 columns by 58 rows).

In the design of the GSO brain scanner we considered the advantages of using the existing electronics from previous NaI(Tl)-based systems from UGM Medical Systems. As first described in [11], the output from each PMT is digitized at short intervals (currently 40 ns) using flash analog-to-digital converters (ADC). Simultaneously the analog output is summed in small groups, called trigger channels and the output of each trigger channel is routed to a constant fraction discriminator (CFD). The very short output signals (4 ns) from the CFDs are 'or-ed' together before going to coincidence circuits. Only the electronics prior to the coincidence circuits need to be designed for high speed, since the count-rate after the coincidence circuit is much lower. After a coincidence is detected, the output signals from the ADCs are summed in order to integrate the light emitted from the scintillation process, and those digital summed outputs, corresponding to two events in coincidence, are processed further to determine the position in the respective areas of the detector. Note that the position determination does not occur for every event, but only those in coincidence, and it does not occur for every group of PMTs as is customary in block designs. Instead, two position calculating circuits are used in parallel for all events. This simplifies the electronics yet allows us to use relatively sophisticated methods to accurately determine the position and energy of each event. For each event, a peak PMT is identified and the event position and

energy are calculated using a 'local centroid' method [12] after the digitized PMT signals are first corrected for gain using a calibration lookup table. At the same time the amplitudes are modified based partly on the total energy signal in a process traditionally carried out in non-linear preamplifiers. After the event position and energy are calculated, both energy and position are corrected for local variations. The spatial-linearity and spatially-varying energy corrections are common for Anger cameras.

The application to GSO detectors required only a few modifications, while maintaining the same architecture and bus structure. The most important was the increase in clock frequency from 25 MHz to 50 MHz. This has the effect of doubling the count-rate capability for processing coincidence events from 700 kcps to 1.5 Mcps, provides generous headroom for the range of count-rates expected to be encountered. In addition, the faster clock speed increases the sampling rate of the ADCs from 40 ns to 20 ns, which is needed with the faster GSO signal. Measurements of energy resolution at a sampling rate of 20 ns have been taken.

Integration time (ns)	Energy Resolution
100	17.2%
140	12.5%
180	11.4%
220	10.4%

Table 1. Integration time vs. energy resolution for GSO using digital sampling electronics with a 50 MHz clock.

The energy resolution at 220 ns matches the result (10%) presented in Section 2, which was taken with a charge integrating ADC. There is some loss of energy resolution at 140 ns due partly to the fact that the trigger, which defines the start of integration, has a 40 ns uncertainty. The final version of the electronics will reduce this uncertainty to 20 ns. This should lead to better results with short integration times for the completed system. We are also testing a pulse shaping circuit to shorten the tail of the scintillation pulse [13], to further improve energy resolution for short integration times.

4. PERFORMANCE SIMULATIONS

A rigorous approach is being taken to optimize the system operation using a combination of three Monte Carlo simulation programs. The first program *Scatter Simulation* is based upon EGS4 [14,15] and is used to calculate Trues (T) and Scatter (Sc) events, depending upon the distribution of activity in the phantom, and the properties of the scanner. The β+ decay is simulated by two back-to-back photons, each with 511 keV, neglecting the positron range and the small non-colinearity of the photon pairs. Moreover, we restrict the simulation to Rayleigh and Compton scattering, the latter being the predominant interaction the photons undergo at these energies. An event is considered as 'true' or unscattered when neither of the two photons is deflected, and is considered as 'scatter' when one or both photons are scattered. The Monte Carlo simulations are used to determine the interaction probability for the photon transport, excluding the detection probability within the crystals and energy resolution. Here we use the results in the form of a look up table from a second Monte Carlo simulation program *Detector Simulation* [16] to determine the detection probabilities and energy deposition for the selected scintillation crystal.

The basic geometric elements of the *Scatter Simulation* program are planes and spheres, which are used to model the gantry, detector crystal, shielding and septa. Simple phantoms consisting of water-filled cylinders can easily be generated. In order to compare the simulated data with the measured data, however, we need to consider dead-time, due to both the detector and the electronics. Our dead-time model [17,18] accounts for the detailed effects of pre- and post-pileup, as well as triggering and other factors of electronic dead-time. This model is incorporated into the third program *Count-rate Simulation*, which calculates system dead-time and randoms as a function of activity.

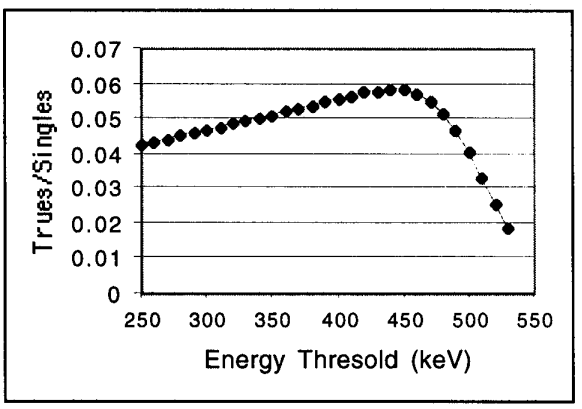

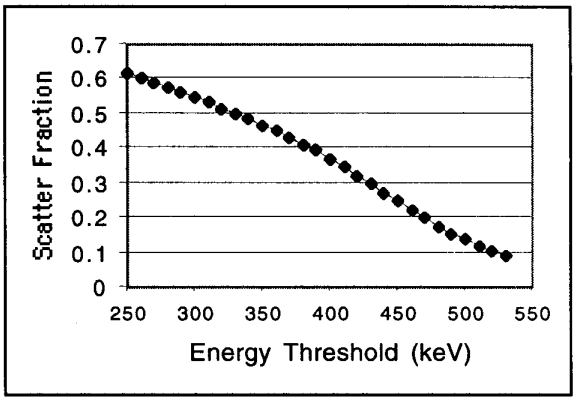

Figure 4. Results from the *Scatter Simulation* program for NEMA phantom.

Figure 4 shows the results from the *Scatter Simulation* program. At a threshold of 450 keV the scatter fraction is about 25%. Above 450 keV, the Trues/Singles ratio decreases, and the Trues decrease, as well, since the program accounts for the broadening due to energy resolution.

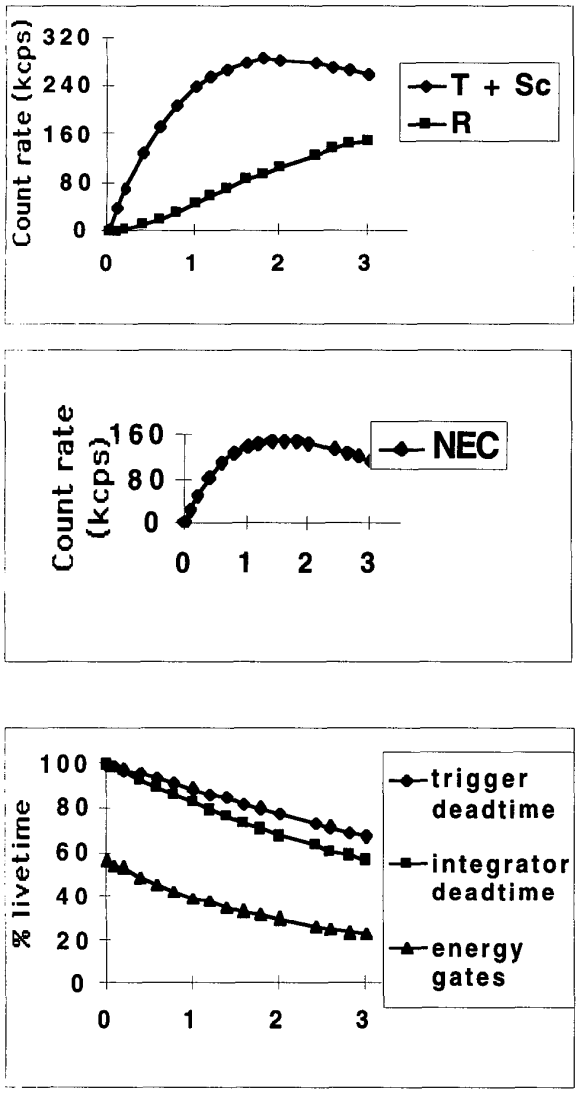

Figure 5. Results from the *Count-rate Simulation* program for a NEMA phantom in the GSO brain scanner. The scatter fraction predicted from the *Scatter Simulation* program is 25%. These simulations assume 2τ = 6 ns, an integration time of 120 ns, and an energy window of 450 –570 keV. Note that the causes of dead-time (bottom plot) are sequential, but represent individual, not cummulative effects. Also, all values correspond to the coincidence live-time rate; in particular, the energy gate live-time of 58% at low activity corresponds to an acceptance of 76% for each detector.

For the simulations shown in Figure 5 we used a conservative estimate of 14% energy resolution for an integration time of 120 ns. The system is assumed to have 15 coincidence triggers, each representing 3 columns of PMTs, with an overlap of 1 column [1,19]. A relatively low trigger threshold of 310 keV is used, to ensure that events sharing light between two trigger channels are not lost. This increases the energy gate rejection rate (even at low activity) since we use an energy window of 450–570 keV. We based this decision on our experience with the NaI(Tl) detector, however, it is possible that the trigger threshold can be raised in actual operation with the GSO detector. Alternatively, we can increase the number of triggers from 18 to 36 (using an overlap of 2 columns). This will allow us to raise the trigger threshold, thus, reducing the energy gate dead-time, and will decrease the trigger dead-time, as well.

The simulations in Figure 5 predict a maximum NEC rate of about 160 kcps at about 1.5 mCi (55 MBq) in the field-of-view. The random fraction (Randoms/Trues) is about 35% at this activity. The major cause of dead-time is due to event pile-up that results in energy gate rejection. For example, at 1.5 mCi, energy gate rejection leads to a loss of 40% (relative to the live-time at low activity). This loss is determined by the fundamental design of the detector, and includes the effects of the LRF and size of the 7-PMT array used for event positioning. However, there is also a significant dead-time due to the electronics, which were originally designed for the lower count-rate requirements of the NaI(Tl) systems. The combination of the effects of trigger dead-time and integration dead-time leads to an additional loss of 40%. This loss can potentially be reduced in the future with faster electronics.

4. DISCUSSION

A new scanner is being constructed, based upon a GSO detector. GSO was chosen because it has good combination of stopping power, fast decay, and light output. At first glance, the light output seems relatively low compared to NaI(Tl) and LSO, but its energy resolution is better than LSO (or LGSO) and it is as good as NaI(Tl) with pulse clipping. For a septa-less system with a large axial FOV, energy resolution is an important feature. The light output of GSO is also sufficient to achieve good spatial resolution using an Anger-type detector design. Using a simulation program, a light-guide was designed to optimize the performance of a detector using 4-mm crystals and 39-mm PMTs. Very good crystal identification was demonstrated experimentally, in agreement with the simulation.

System spatial resolution is expected to be 3-3.5 mm, considering the width of the coincidence line spread function (1/2 crystal width), and the effects of positron range and gamma ray non-colinearity. The error due to non-colinearity is minimized by the small diameter of the system, (42 cm), and the parallax error is minimized by using relatively thin crystals (10-mm). For a system based on discrete crystals, the spatial resolution is normally limited by the sampling, unless some type of detector motion is used (e.g. wobbling). Since the crystals are not sub-divided into blocks nor are they

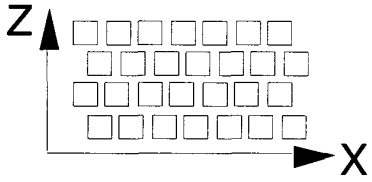

Figure 6. Staggered orientation of crystals

aligned with the PMTs, we have more .flexibility in the crystal configuration, and have decided to stagger adjacent rows by

one-half crystal width. This means that we can reduce the radial (or angular) sampling by a factor of two for the in-plane lines-of-response, at the expense of out-of-plane sampling. The optimal choice of sampling depends on the method of 3D reconstruction, which is currently under investigation.

The system has a detector diameter of 42 cm and an axial FOV of 25 cm. A total of 288 PMTs are required with 18,560 crystals. A *Scatter Simulation* program and *Count-rate Simulation* program were used together to estimate the performance of the complete system. The system will have a sensitivity of 1.2 Mcps/μCi/ml (for NEMA phantom) with a scatter fraction of 25%, using an energy window of 450–570 keV. The peak NEC of 160 kcps is reached at 1.5 mCi in the FOV. With a narrow coincidence time window (6 ns), which is appropriate for a fast scintillator such as GSO, the random fraction will be less of a limitation than system dead-time. The major cause of dead-time is due to pulse pile-up and is limited by the Anger-type detector design and the size of the PMT cluster (7 PMTs) used for event positioning. It would be possible to tune the light-guide and LRF for a smaller PMT, but we feel that the 39-mm PMT offers a practical trade-off between total system cost and count-rate performance. Although we also expect there to be significant losses due to electronic dead-time, it will be possible to reduce these effects through improvements to the acquisition electronics.

Through a combination of experimentation and computer simulations, we have shown that GSO can be used to design a high performance PET scanner. Although more expensive than NaI(Tl) and BGO, GSO is much less expensive than LSO. Equally important, the GSO crystals (from Hitachi Chemical Inc.) have very uniform performance. All crystals (which have been delivered) undergo individual testing before being glued to the light-guide. We have found that the variation in light output among a large sample of these crystals is only ±5% (standard deviation). Thus, we can expect that the performance of the complete system will be comparable to that of the small detector module, which was presented. The system is under construction at this time, and will be completed in several months.

ACKNOWLEDGEMENTS

This work was supported by the Counter Drug Technology Assessment Center (CTAC), an office within the Office of National Drug Control Policy, and by the U.S. Department of Energy grant no. DE-FG02-88ER60642. L. Adam was also supported in part by the Cassen Fellowship from the Society of Nuclear Medicine.

The authors gratefully acknowledge the team of engineers and scientists at ADAC UGM for their contributions to the development of this scanner.

REFERENCES

[1] Freifelder R, Karp JS, Geagan M, Muehllehner G, "Design and performance of the HEAD PENN-PET scanner," *IEEE Trans Nucl Sci* 41: 1436-1440, 1994.

[2] Karp JS, Freifelder R, Geagan MJ, Muehllehner G, Kinahan PE, Lewitt RM, Shao, L, "3D imaging characteristics of the HEAD PENN-PET scanner," *J Nuc Med* 38: 636-643, 1997.

[3] Takagi K, Fukazawa T, "Cerium-activated Gd_2SiO_5 single crystal scintillator," *App Phys Lett* 42: 43-45, 1983.

[4] Dahlbom M, Mandelkem MA, Hoffman EJ et al., "Hybrid HgI_2-GSO detector for PET," *IEEE Trans Nucl Sci* 32: 533-537, 1985.

[5] Eriksson L, Bohm C, Kesselberg M, et al., "A four ring positron camera system for emission tomography of the brain," *IEEE Trans Nucl Sci* 29: 539-543, 1985.

[6] Melcher CL, Schmand, M, Eriksson M, Eriksson L, Casey M, Nutt R. Scintillation properties of LSO:Ce Boules," *Conference Record of the 1998 IEEE Nuclear Science Symposium and Medical Imaging Conference*.

[7] Kurashige K, Kurata Y, Ishibashi H, Susa K., "Surface polish of GSO scintillators using chemical processes," *IEEE Trans Nucl Sci* .45: 522-524, 1998.

[8] M. Moszynski, M. Kapusta, D. Wolski, M. Szawlowski, and W. Klamra, "Energy Resolution of Scintillation Detectors Readout with Large Area Area Avalanche Photodiodes and Photomultipliers," *IEEE Trans. Nucl. Sci.*, 45: 472-477, 1998.

[9] Suleman S, Karp JS, Freifelder, R, Liu F, "Optimizing the performance of a PET detector using discrete GSO crystals on a continuous lightguide," *Conference Record of the 1999 IEEE Nuclear Science Symposium and Medical Imaging Conference*,

[10] Burnham CA, Kaufman DE, Chesler DA, Stearns CW, Wolfson DR, Brownell GL, "Cylindrical PET Detector Design," *IEEE Trans Nucl Sci* 35: 675-679, 1988.

[11] Karp JS, Muehllehner G, Beerbohm D, Mankoff D, "Event localization in a continuous scintillation detector using digital processing," *IEEE Tran Nucl Sci* NS-33:550-555, 1986.

[12] Karp JS, Mankoff DA, Muehllehner G, "A position-sensitive detector for use in positron emission tomography," *Nucl Instr Meth* A273:891-897, 1988.

[13] Freifelder R, Karp JS, Wear JA, Lockyer NS, Newcomer FM, Surti S, Van Berg R, "Comparison of multi-pole shaping and delay-line clipping pre-amplifiers for position sensitive NaI(Tl) detectors," *IEEE Tran Nucl Sci* 45: 1138-1143, 1998.

[14] Nelson WR, Hirayama H, and Rogers DWO, "The EGS4 code system," SLAC-Report-265, Stanford University, Stanford, 1985.

[15] Adam LE, Karp JS, Brix G, "Investigation of scattered radiation in 3D whole-body positron emission tomography using Monte Carlo simulations," *Phys. Med. Biol.*,(in press).

[16] Karp JS, Muehllehner G, "Performance of a position-sensitive scintillation detector," *Phys Med Biol* 30:643-655, 1985.

[17] Mankoff DA, Muehllehner G, Karp JS, "The high countrate performance of a two-dimensionally position-sensitive detector for positron emission tomography," *Phys Med Biol* 34:437-456, 1989.

[18] Wear JA, Karp JS, Freifelder R, Mankoff DA, Muehllehner G, "A model of the high count rate performance of NaI(Tl)-based detectors," *IEEE Tran Nucl Sci* 45: 1231-1237, 1998.

[19] Mankoff DA, Muehllehner G, Miles G, "A local coincidence triggering system for PET tomographs composed of large-area continuous position-sensitive detectors," *IEEE Trans Nucl Sci.* 37:730-736, 1990.